Title

Lower PDL1, PDL2, and AXL Expression on Lung Myeloid Cells Suggests Inflammatory Bias in Smoking and Chronic Obstructive Pulmonary Disease.

Journal

American Journal of Respiratory Cell and Molecular Biology, 63(6)

ISSN

1044-1549

Authors

Vasudevan, Sreelakshmi
Vásquez, Joshua J
Chen, Wenxuan
et al.

Publication Date

2020-12-01

DOI

10.1165/rcmb.2020-0085oc

Peer reviewed

ORIGINAL RESEARCH

Lower PDL1, PDL2, and AXL Expression on Lung Myeloid Cells Suggests Inflammatory Bias in Smoking and Chronic Obstructive Pulmonary Disease

Sreelakshmi Vasudevan[1,2*], Joshua J. Vásquez[2,3*], Wenxuan Chen[1,2,3], Brandon Aguilar-Rodriguez[2,3], Erene C. Niemi[1,4], Siyang Zeng[1,2], Whitney Tamaki[3], Mary C. Nakamura[1,4], and Mehrdad Arjomandi[1,2,5]

[1]Medical Service, San Francisco Veterans Affairs Healthcare System, San Francisco, California; [2]Division of Pulmonary, Critical Care, Allergy, and Sleep Medicine, [3]Division of Experimental Medicine, [4]Division of Rheumatology, and [5]Division of Occupational and Environmental Medicine, Department of Medicine, University of California at San Francisco, San Francisco, California

ORCID IDs: 0000-0002-7165-5739 (J.J.V.); 0000-0002-0116-9217 (M.A.).

Abstract

Lung myeloid cells are important in pulmonary immune homeostasis and in the pathogenesis of chronic obstructive pulmonary disease (COPD). Multiparameter immunophenotypic characterization of these cells is challenging because of their autofluorescence and diversity. We evaluated the immunophenotypic landscape of airway myeloid cells in COPD using time of flight mass cytometry. Cells from BAL, which were obtained from never-smokers ($n = 8$) and smokers with ($n = 20$) and without ($n = 4$) spirometric COPD, were examined using a 44-parameter time of flight mass cytometry panel. Unsupervised cluster analysis was used to identify cellular subtypes that were confirmed by manual gating. We identified major populations of $CD68^+$ and $CD68^-$ cells with 22 distinct phenotypic clusters, of which 18 were myeloid cells. We found a higher abundance of putative recruited myeloid cells ($CD68^+$ classical monocytes) in BAL from patients with COPD. $CD68^+$ classical monocyte population had distinct responses to smoking and COPD that were potentially related to their recruitment from the interstitium and vasculature. We demonstrate that BAL cells from smokers and subjects with COPD have lower AXL expression. Also, among subjects with COPD, we report significant differences in the abundance of $PDL1^{high}$ and $PDL2^{high}$ clusters and in the expression of PDL1 and PDL2 across several macrophage subtypes suggesting modulation of inflammatory responses. In addition, several phenotypic differences in BAL cells from subjects with history of COPD exacerbation were identified that could inform potential disease mechanisms. Overall, we report several changes to the immunophenotypic landscape that occur with smoking, COPD, and past exacerbations that are consistent with decreased regulation and increased activation of inflammatory pathways.

Keywords: lung immunology; COPD; macrophages; mass cytometry; COPD exacerbations

(Received in original form March 2, 2020; accepted in final form September 11, 2020)

*These authors contributed equally to this work.

Supported by funds from the Tobacco-related Disease Research Program of the University of California (28FT-0020 [S.V.]; T29IR0715 [M.A.]); the Department of Defense Congressionally Directed Medical Research Programs Peer-reviewed Medical Research Program Discovery Award (W81XWH-20-1-0158 [M.A.]); the National Center for Advancing Translational Sciences, National Institutes of Health, through University of California, San Francisco–Clinical and Translational Science Institute (CTSI) grants (UL1 TR000004 and UL1 TR001872); the U.S. National Institutes of Health (K01HL140804–01A1, UM1 AI126611, U19 AI096109, R21 AI116295, and R33 AI116025 [J.J.V.]); University of California, San Francisco, Gladstone Institute of Virology and Immunology Center for Acquired Immunodeficiency Syndrome Research (P30-AI027763 [J.J.V.]); the American Foundation for Acquired Immunodeficiency Syndrome Research Institute for Human Immunodeficiency Virus Cure Research (109301-59-RGRL [J.J.V.]); the Robert Wood Johnson Foundation Harold Amos Medical Faculty Development Program (J.J.V.); the University of California, San Francisco, Nina Ireland Program for Lung Health (J.J.V.); the Diabetes Research Center (DRC) Center grant (National Institutes of Health grant P30 DK063720 [to University of California, San Francisco, Flowcore] and National Institutes of Health grant S10 1S10OD018040-01 [for time of flight mass cytometry 2 instrument]); Department of Veterans Affairs Biomedical Laboratory Research and Development Merit award (BX002994 [M.C.N.]); the National Institute of Arthritis and Musculoskeletal and Skin Diseases (awards R01AR066735 and P30AR070155); and the Russell/Engelman Rheumatology Research Center at University of California, San Francisco (M.C.N.).

Author Contributions: Conceived and designed the current manuscript study: S.V., J.J.V., and M.A. Developed study protocols: S.V., J.J.V., W.C., B.A.-R., E.C.N., and M.A. Collected data: S.V., J.J.V., W.C., B.A.-R., E.C.N., S.Z., and M.A. Analyzed and interpreted data: S.V., J.J.V., S.Z., W.T., M.C.N., and M.A. Prepared and edited the manuscript: S.V., J.J.V., S.Z., M.C.N., and M.A. Obtained funding: S.V., J.J.V., M.C.N., and M.A.

Correspondence and requests for reprints should be addressed to Joshua J. Vásquez, M.D., Division of Experimental Medicine, Zuckerberg San Francisco General Hospital, Building 3, Room 603, Mailbox 1234, 1001 Potrero Avenue, San Francisco, CA 94143. E-mail: joshua.vasquez@ucsf.edu.

This article has a data supplement, which is accessible from this issue's table of contents at www.atsjournals.org.

Am J Respir Cell Mol Biol Vol 63, Iss 6, pp 780–793, Dec 2020

Originally Published in Press as DOI: 10.1165/rcmb.2020-0085OC on September 11, 2020
Internet address: www.atsjournals.org

Clinical Relevance

This study provides novel evidence using mass cytometry for the impact of smoking and chronic obstructive pulmonary disease (COPD) on airway myeloid cells, including decrease in regulatory proteins such as PDL1, PDL2, and AXL, which may contribute to chronic inflammation in COPD. These findings expand the field of COPD and myeloid immunobiology by establishing a framework to evaluate airway myeloid subpopulations during disease progression or response to treatment.

Chronic obstructive pulmonary disease (COPD) affects over 250 million people and is a leading cause of death worldwide (1). Pulmonary immune cells, including myeloid cells, are believed to play an important role in its homeostasis (2). In COPD, prolonged exposure to tobacco smoke causes chronic inflammation in airways and alters the phenotype and function of lung myeloid cell populations, which likely contributes to the pathogenesis of COPD (3).

Previous *in vitro* and animal studies have documented the diversity and plasticity of lung myeloid cells. However, the evaluation of myeloid phenotypes in the lungs of individuals with COPD has been limited, in part, because of technical challenges including intense autofluorescence, which restricts the use of fluorescence-based immunological assays such as flow cytometry and microscopy for characterizing these cells, particularly in active smokers (4, 5). Although transcriptional characterization of lung myeloid phenotypes has been performed, multiparameter single-cell proteomic analyses of these cells remain limited.

The goal of this study was to determine the influence of smoking and COPD on the composition of lung myeloid cells obtained by BAL sampling of airways. We used time of flight mass cytometry (CyTOF)-based immunophenotypic analysis of a 39-parameter myeloid cell–focused panel, targeting markers that inform the potential for cellular activation, inhibition, migration, and/or functionality. We hypothesized that myeloid cells obtained by BAL from patients with COPD would express markers suggestive of dysregulation, immune inhibition, and recruitment from the peripheral circulation. In addition, we posited that dysregulated myeloid phenotypes found in the BAL would be more pronounced among those patients with COPD with a history of moderate and severe exacerbations. To address these hypotheses, we used CyTOF-based immune profiling of myeloid cells from the BAL of subjects with and without a history of smoking or COPD to identify specific myeloid subtypes and immune expression profiles associated with smoking and COPD.

Methods

Additional study methods are detailed in the data supplement.

Study Design

This was an observational study of 32 subjects with and without a history of smoking or spirometric COPD. Eligible subjects were characterized using health and symptom questionnaires and spirometry before and after bronchodilator administration followed by bronchoscopy with BAL, as previously described (6). The BAL return volume and cell characteristics assessed by cytospin are provided in Table 1. Cells from BAL were counted and viably cryopreserved in liquid nitrogen.

Study subjects. Subjects aged 45–80 years were recruited between 2014 and 2018 and characterized on the basis of smoking status and presence of spirometric COPD (*see* Figure E1 in the data supplement). Never-smokers had to have less than 1 pack-year history of tobacco use with no smoking in the past 20 years and normal spirometry ($FEV_1/FVC \geq 0.70$ and $FEV_1 > 80\%$ of predicted value by the Crapo reference equation) (7). Smokers had to have ⩾20 pack-years history of smoking. Subjects were considered former smokers if they had not smoked tobacco for more than 1 year or were considered current smokers if they had smoked at least one cigarette per day in the preceding 3 months. Subjects who had not smoked tobacco for 3 months or more and less than 1 year were excluded. COPD was defined by spirometry using the Global Initiative on Obstructive Lung Disease (GOLD) criteria as $FEV_1/FVC < 0.70$. Subjects with COPD GOLD stage 1 disease ($FEV_1 \geq 80\%$ of predicted value) were excluded to increase the likelihood of identifying clinically meaningful differences in marker expression. Subjects with COPD were further categorized as exacerbators if they had a history of at least one exacerbation of moderate or greater severity within the 3 years preceding the enrollment, which was quantified using a clinical exacerbation questionnaire (data supplement) and detailed medical chart review. The exacerbation severity was categorized on the basis of whether the subjects required ICU care (very severe), hospitalization without ICU care (severe), acute care or emergency room visits without hospitalization (moderate), or no in-person healthcare visits (mild).

Individuals with the following histories or conditions were excluded: asthma, systemic chemotherapy, radiation therapy to the chest, autoimmune diseases, hereditary or acquired immune system disorders, active hepatitis B or C, intravenous drug use for more than 1 year or within 30 years, and inhaled marijuana, crack, or methamphetamine use. All subjects were interviewed and examined by a pulmonologist to evaluate their safety for undergoing bronchoscopy.

The institutional review board at the University of California, San Francisco (UCSF) and the San Francisco Veterans Affairs Healthcare System Research and Development Committee approved the protocols and performance of this study. Written informed consent was obtained from all subjects.

Mass Cytometry

Sample preparation and staining. Cryopreserved cells were thawed and counted, and samples with less than 50% viability were excluded. The mean viability of included samples was 82.3% with 10.3% SD. The qualified samples were live-dead stained with Cell-ID Cisplatin (201064; Fluidigm) at a dilution of 1:2,000 for 5 minutes. Cells were quenched, washed with CyPBS (MB-008; Rockland) containing 0.1% BSA (CyFACS) and fixed with 1.6% paraformaldehyde for 10 minutes. Cells were barcoded with 10-plex Palladium barcoding kit (UCSF core facility) according to manufacturer's instructions, pooled together, and blocked with a serum cocktail containing human, rat, and mouse serums. One aliquot of the blocked sample was kept aside as an unstained sample for quality control. The remaining cells were labeled with surface antibodies for 45 minutes. Cells were subsequently permeabilized with

Table 1. Demographics and Clinical Characteristics*

	All Subjects	No COPD	COPD	Nonexacerbator	Exacerbator
Basic characteristics					
Subjects, *n* (%)	32	12 (37.5)	20 (62.5)	13/20 (65.0)	7/20 (35.0)
Age, yr, mean ± SD	64.4 ± 6.1	62.5 ± 5.1	65.0 ± 6.5	64.6 ± 6.1	65.5 ± 7.5
Sex, F, *n* (%)	7 (22)	3 (25)	4 (20)	1 (8)	3 (43)
Height, cm, mean ± SD	176 ± 8	177 ± 9	175 ± 7	177 ± 6	172 ± 7
BMI, kg/m^2, mean ± SD	27.4 ± 6.8	27.4 ± 9.2	27.6 ± 4.9	26.5 ± 4.47	29.8 ± 5.3
Smoking status, *n* (%)					
Never-smokers	8 (25)	8 (67)	0 (0)	0 (0)	0 (0)
Former smokers	9 (28)	0 (0)	9 (45)	5 (39)	4 (57)
Current smokers	15 (47)	4 (33)	11 (55)	8 (62)	3 (43)
Smoking history, pack-years, median (IQR)	40.0 (24.8 to 47.8)	2 (0 to 38.8)	44.5 (35.5 to 56.0)	43 (37 to 64.5)	45 (37.5 to 47.5)
Had history of moderate or severe exacerbations,* *n* (%)	7 (21.8)	0 (0)	7 (35.0)	0 (0)	7 (100)†
Severity of exacerbations,* *n* (%)	10 (31.3)	0 (0)	10 (50.0)	3 (23.1)	7 (100)
Mild	3 (9.4)	0 (0)	3 (15.0)	3 (23.1)	0 (0)
Moderate	6 (18.8)	0 (0)	6 (30.0)	0 (0)	6 (85.7%)†
Severe	3 (9.4)	0 (0)	3 (15.0)	0 (0)	3 (42.9)
Very severe	1 (3.1)	0 (0)	1 (5.0)	0 (0)	1 (14.3)
Number of exacerbations,* mean ± SD	1.0 ± 1.8	0 ± 0	1.6 ± 2.0†	0.9 ± 1.7	2.9 ± 2.0†
Median (IQR)	0 (0 to 1.3)		0.5 (0 to 2.3)	0 (0 to 0)	2.0 (1.5 to 4.0)
Mild	0.3 ± 1.2	0 ± 0	0.6 ± 1.4	0.9 ± 1.7	0 ± 0
	0 (0 to 0)		0 (0 to 0)	0 (0 to 0)	
Moderate	0.5 ± 1.2	0 ± 0	0.8 ± 1.5	0 ± 0	2.1 ± 2.0†
	0 (0 to 0)		0 (0 to 1.0)		2.0 (1.0 to 2.5)
Severe	0.1 ± 0.4	0 ± 0	0.2 ± 0.5	0 ± 0	0.6 ± 0.8†
	0 (0 to 0)		0 (0 to 0)		0 (0 to 1.0)
Very severe	0.03 ± 0.2	0 ± 0	0.1 ± 0.2	0 ± 0	0.1 ± 0.4
	0 (0 to 0)		0 (0 to 0)		0 (0 to 0)
Airflow indices, mean ± SD					
FEV_1% predicted	73 ± 23	96 ± 17	59 ± 10†	59 ± 9	60 ± 13
FVC% predicted	87 ± 19	98 ± 19	80 ± 15†	79 ± 16	81 ± 13
FEV_1/FVC, %	65 ± 12	77 ± 4	58 ± 10†	58 ± 10	57 ± 10
FEV_1/FVC% predicted	84 ± 16	99 ± 5	75 ± 12†	75 ± 12	74 ± 13
Reversibility in FEV_1, ml	95 ± 125	73 ± 91	109 ± 143	71 ± 144	180 ± 117
	100 (18 to 170)	95 (−3 to 145)	100 (28 to 200)	90 (20 to 110)	200 (100 to 280)
Reversibility in FEV_1, %	5.8 ± 8.3	2.6 ± 3.0	7.7 ± 9.8	4.8 ± 9.4	13.0 ± 8.9
	4.1 (0.6 to 7.7)	3.8 (−0.1 to 4.4)	5.5 (1.4 to 12.3)	4.5 (0.8 to 6.0)	16.3 (6.5 to 18.9)
Reversibility in FEV_1, *n* (%)	4 (12.5)	0 (0)	4 (20.0)	1 (7.7)	3 (42.9)
Clinical characteristics					
GOLD stage, *n* (%)					
0	12 (37.5)	12 (100)	—	—	—
1	0 (0)	—	0 (0)	0 (0)	0 (0)
2	16 (50.0)	—	16 (80.0)	11 (84.6)	5 (71.4)
3	4 (12.5)	—	4 (20.0)	2 (15.4)	2 (28.6)
4	0 (0)	—	0 (0)	0 (0)	0 (0)
Medications, *n* (%)					
ICS	4 (12.5)	0 (0)	4 (20.0)	0 (0)	4 (57.1)†
LABA	1 (3.1)	0 (0)	2 (10.0)	0 (0)	2 (28.6)†
LAMA	4 (12.5)	0 (0)	4 (20.0)	2 (15.4)	2 (28.6)
SABA	7 (21.9)	0 (0)	7 (35.0)†	4 (30.8)	3 (42.9)
SAMA	4 (12.5)	0 (0)	4 (20.0)	1 (7.7)	3 (42.9)
Oral steroid	0 (0)	0 (0)	1 (5.0)	0 (0)	1 (14.3)
Antihistamine	2 (6.3)	0 (0)	2 (10.0)	2 (15.4)	0 (0)
SABA + SAMA	1 (3.1)	0 (0)	1 (5.0)	0 (0)	1 (14.3)
ICS + LABA	2 (6.3)	0 (0)	2 (10.0)	0 (0)	2 (28.6)†
BAL characteristics, mean ± SD					
Return volume, ml	111.9 ± 5.3	133.9 ± 5.8	98.7 ± 6.0†	99.7 ± 7.8	96.9 ± 10.0
Total immune cells, 10^4/ml	29.83 ± 4.41	31.37 ± 8.34	28.90 ± 5.15	28.06 ± 4.70	30.46 ± 12.53
Total macrophages, 10^4/ml	22.41 ± 4.08	17.00 ± 7.63	25.66 ± 4.94	24.28 ± 4.70	28.23 ± 11.70
Total neutrophils, 10^4/ml	0.89 ± 0.41	0.29 ± 0.15	1.25 ± 0.58	1.64 ± 0.87	0.54 ± 0.35
Total eosinophils, 10^4/ml	0.23 ± 0.09	0.14 ± 0.06	0.28 ± 0.14	0.38 ± 0.20	0.08 ± 0.06
Total lymphocytes, 10^4/ml	1.17 ± 0.32	0.30 ± 0.1	1.69 ± 0.44†	1.77 ± 0.62	1.54 ± 0.59

Definition of abbreviations: BMI = body mass index; COPD = chronic obstructive pulmonary disease; FEV_1 = forced expiratory volume in 1 second; FVC = forced vital capacity; GOLD = Global Initiative on Obstructive Lung Disease; ICS = inhaled corticosteroid; IQR = interquartile range; LABA = long-acting β-agonist; LAMA = long-acting muscarinic antagonist; SABA = short-acting β-agonist; SAMA = short-acting muscarinic antagonist.
Reference equations: measures of pulmonary function and percentage predicted of normal values were calculated using Crapo predicted formulas.
Reversibility was defined as ⩾12% and ⩾200 ml increase in FEV_1 after bronchodilators administration.
*Cumulative exacerbation episodes 3 years preceding enrollment. The exacerbation severity was categorized on the basis of whether the subjects required ICU care (very severe), hospitalization without ICU care (severe), acute care or emergency room visits without hospitalization (moderate), or no in-person healthcare visits (mild).
†*P* value < 0.05 when compared with no COPD in case of COPD column and nonexacerbator in case of exacerbator column.

MaxPar Perm-S Buffer (201066; Fluidigm) and then blocked with serum cocktail for 20 minutes. Intracellular antibody labeling was performed for 45 minutes. Cells (stained and unstained) were then labeled with Cell-ID Intercalator-Ir (201192A; Fluidigm) overnight. Cells were analyzed on a CyTOF2 mass cytometer (UCSF single-cell analysis core) after the addition EQ four element calibration beads (1:10, 201078; Fluidigm), and data were collected as flow cytometry standard (FCS) files.

Data deconvolution and analysis. Acquired data were normalized and debarcoded using the Matlab-based open access package (https://github.com/nolanlab). High-dimensional data analysis was performed on $CD45^+$ cells from all samples after the exclusion of dead cells and debris. The data underwent Arcsinh (cytofAsinh) transformation and tSNE dimension reduction using default settings (t-distributed stochastic neighbor embedding [tSNE] perplexity, 30; tSNE max iterations, 1,000; tSNE seed, 42) on the cytofkit package (8). Clusters of $CD45^+$ immune cells were identified by unsupervised analysis of all other markers (Table 2) using the Rphenograph (k = 30) cytofkit package. Median signal intensities for each marker within distinct clusters were z normalized and then visualized in a heatmap to identify and annotate cell clusters. Unsupervised hierarchical clustering of the heatmap was used to annotate clusters on the basis of dendrograms and marker expression. Clusters or cluster-groups were confirmed using manual gating of two-dimensional scatter plots in Cytobank (Cytobank, Inc.). The number of cells contained within an individual cluster, termed "cluster abundance," was evaluated and expressed as a percentage of the total $CD45^+$ cells (Table E1). The expression of markers on each cluster are reported as median intensities. Intercluster relationships were evaluated using isometric feature mapping (ISOMAP) (8) progression analysis (cytofkit) and principal component analysis (PCA). For ISOMAP, samples were down sampled by the ceil method (n = 500/sample) and the global interrelatedness of clusters was visualized by overlaying clusters into ISOMAP dimensions. Subset relatedness was then determined by proximity.

Table 2. List of Mass Cytometry Antibodies and Channels

Channel	Target	Clone Designation	Manufacturer
^{89}Y	CD45	H130	Fluidigm
^{140}Ce	CD8α	RPA-T8	BioLegend
^{142}Nd	CD19	HIB19	Fluidigm
^{142}Nd	CD56	My31.13	BD Biosciences
^{142}Nd	CD66b	80H3	Bio-Rad
^{145}Nd	CD16	3G8	Fluidigm
^{149}Sm	CD141	M80	BioLegend
^{157}Gd	BDCA2	201A	BioLegend
^{160}Gd	CD14	M5E2	Fluidigm
^{168}Er	CD206 (MMR)	15-2	Fluidigm
^{170}Er	CD3	UCHT1	Fluidigm
^{176}Yb	CD1c	L161	BioLegend
^{143}Nd	CD91	A2MR-A2	BD Biosciences
^{147}Sm	TLR8	935166	R&D Systems
^{148}Nd	CD274 (PD-L1)	29E.2A3	Fluidigm
^{154}Sm	CD163	GHI/61	Fluidigm
^{158}Gd	CD284 (TLR4)	HTA125	Fluidigm
^{162}Dy	CD172a (SIRPa)	602411	R&D Systems
^{163}Dy	Galectin-9	9M1-3	Fluidigm
^{164}Dy	TLR7	533707	R&D Systems
^{166}Er	CD200R	Polyclonal	R&D Systems
^{167}Er	AXL	Polyclonal	R&D Systems
^{172}Yb	CD273 (PD-L2)	24F.10C12	Fluidigm
^{174}Yb	HLA-DR	L243	Fluidigm
^{113}In	CD68	Y1/82A	BD Biosciences
^{146}Nd	CD64	10.1	Fluidigm
^{152}Sm	CD36	5-271	Fluidigm
^{159}Tb	CD11c	Bu15	Fluidigm
^{169}Tm	CD169	7-239	BioLegend
^{171}Yb	CD44	IM7	Fluidigm
^{175}Lu	CD71	OKY-9	Fluidigm
^{141}Pr	CD196 (CCR6)	11A9	Fluidigm
^{144}Nd	CD195 (CCR5)	NP-6G4	Fluidigm
^{150}Nd	CD86	IT2.2	Fluidigm
^{153}Eu	CD192 (CCR2)	K036C2	Fluidigm
^{156}Gd	CXCR3	G025H7	Fluidigm
^{161}Dy	CX3CR1	2A9-1	BioLegend
^{165}Ho	CD40	5C3	Fluidigm
^{173}Yb	CD184 (CXCR4)	12G5	Fluidigm

Definition of abbreviations: BDCA2 = blood dendritic cell antigen 2; CX3CR1 = CX3C chemokine receptor 1; HLA-DR = human leukocyte antigen-DR isotype; MMR = macrophage mannose receptor; TLR4 = Toll-like receptor 4.

Data Analysis and Statistics

Clinical data. Distributions of subject characteristics were computed and analyzed. PCA was performed with cluster abundance and marker expressions and was adjusted for age and sex. Resulted principal components were plotted to identify differences in the cluster abundance and marker expression (within clusters) between clinical groups of interest (smoking status, COPD GOLD stages, and history of moderate or severe exacerbations). Regression modeling adjusted for age was performed to examine differences in *1*) the abundance of each cluster and *2*) marker expressions within each cluster. Differences in these parameters were then evaluated between subjects by smoking status. Similar analyses were performed to examine differences by GOLD stage among subjects with COPD compared with never-smokers after adjustment for age and smoking status. Those differences are displayed as parameter estimates with confidence intervals from the regression model for GOLD stages. Differences in cluster abundances and marker expressions were also evaluated among subjects with COPD who had a history of moderate or severe exacerbation, adjusting for age, smoking status, and GOLD stages. Differences by smoking status and exacerbation history are displayed with the distribution of raw data presented as the percentage of cells in each cluster or median intensities with interquartile range. Statistical significance was corrected for multiple comparisons using the Benjamini-Hochberg (BH) method. Results were considered significant if the P values in

the regression models were <0.1 after a BH correction. R software (version 3.5.2; R Foundation for Statistical Computing) was used for data management, analysis, and PCA plots. Figures were generated by GraphPad (Prism version 7.0).

Results

Characterization of Subject

The clinical characteristics of each cohort, including demographics, smoking status and burden, medications, spirometry, and cell characteristics, are listed in Table 1. Overall, BAL cells were obtained from 12 subjects without COPD (eight never-smokers and four current smokers) and 20 subjects with COPD (nine former smokers and 11 current smokers). Seven of the 20 subjects with COPD had history of moderate or severe exacerbations within the 3 years preceding their enrollment in the study and were classified as exacerbators. None of the subjects were on systemic corticosteroid and only four were on inhaled corticosteroid.

Cell-associated Heavy-Metal Contamination in Smokers Impacts the Use of Lanthanum and Cerium Channels for Mass Cytometry of Lung Cells

A myeloid cell–focused mass cytometry panel was designed and optimized to evaluate the phenotype of immune cells in BAL. The performance of metal-labeled antibodies was confirmed for individual markers in each sample on $CD45^+$ cells, $CD3^+$ T cells, non-T cells, $CD68^+$ non-T cells, and $CD68^-$ non-T cells (Figure E2). The distribution of marker expression across clusters were also evaluated by visualization in tSNE space (Figure E3). Prior studies have demonstrated high concentrations of heavy metals in indoor air with environmental tobacco smoke (9). These heavy metals can be used as antibody conjugates in mass cytometry; therefore, as a quality control measure, unstained samples were run from each subject together with the stained sample. Unstained samples revealed contamination with

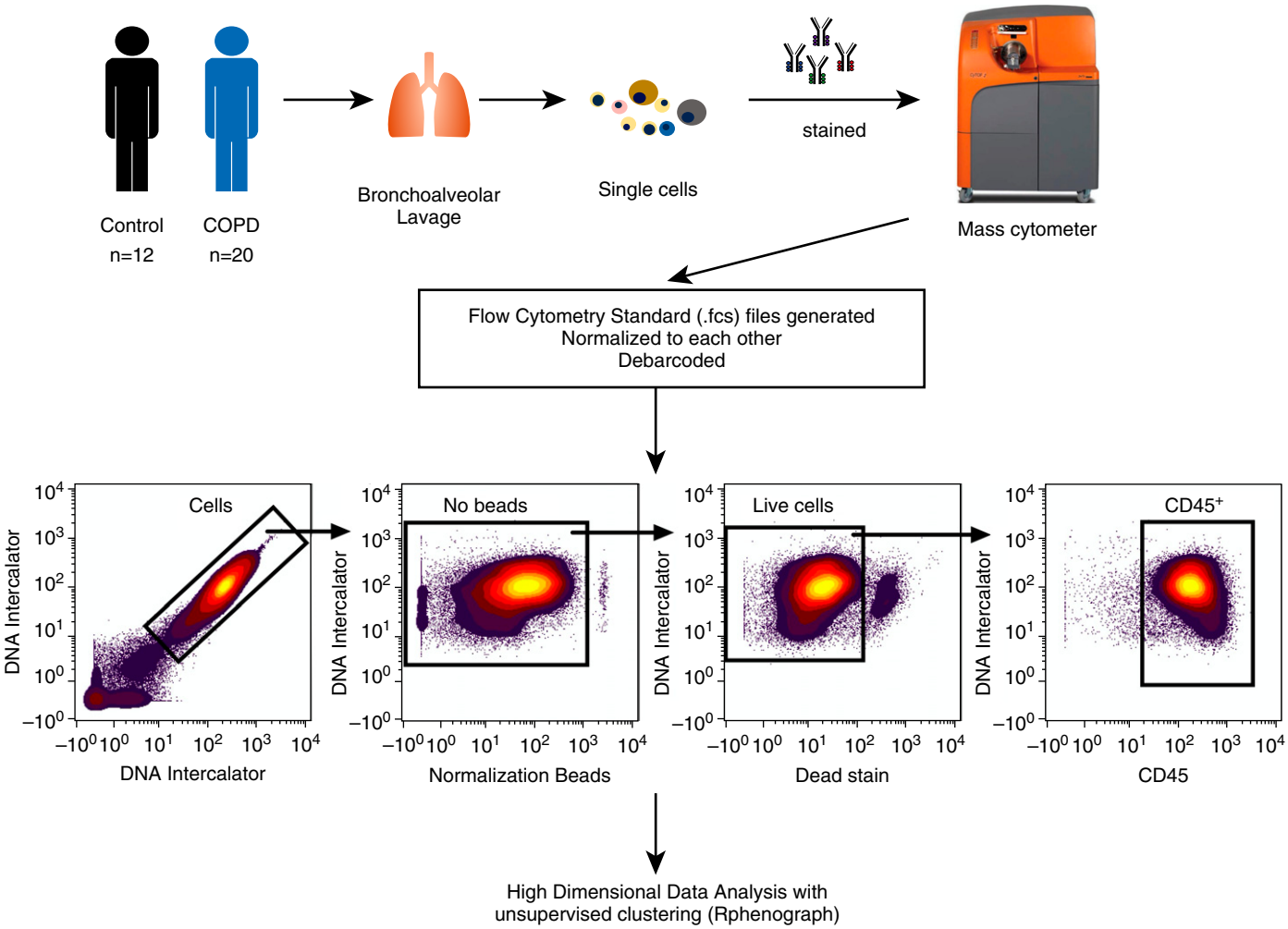

Figure 1. Experimental design and data deconvolution. BAL was performed on subjects without chronic obstructive pulmonary disease (COPD) (control; $n = 12$) and with COPD ($n = 20$), and BAL immune cells were isolated and made into single-cell suspensions. The cells were stained with metal isotope–labeled antibodies and analyzed on a time of flight mass cytometry 2 mass cytometer. Data generated were normalized and debarcoded for data deconvolution and quality control. Cells were identified using DNA intercalator, normalization beads were gated out, live cells were identified by gating out cisplatin (live–dead)-positive cells, and immune cells were gated in using CD45 positivity. The $CD45^+$ cells were used for downstream high-dimensional analysis using Rphenograph.

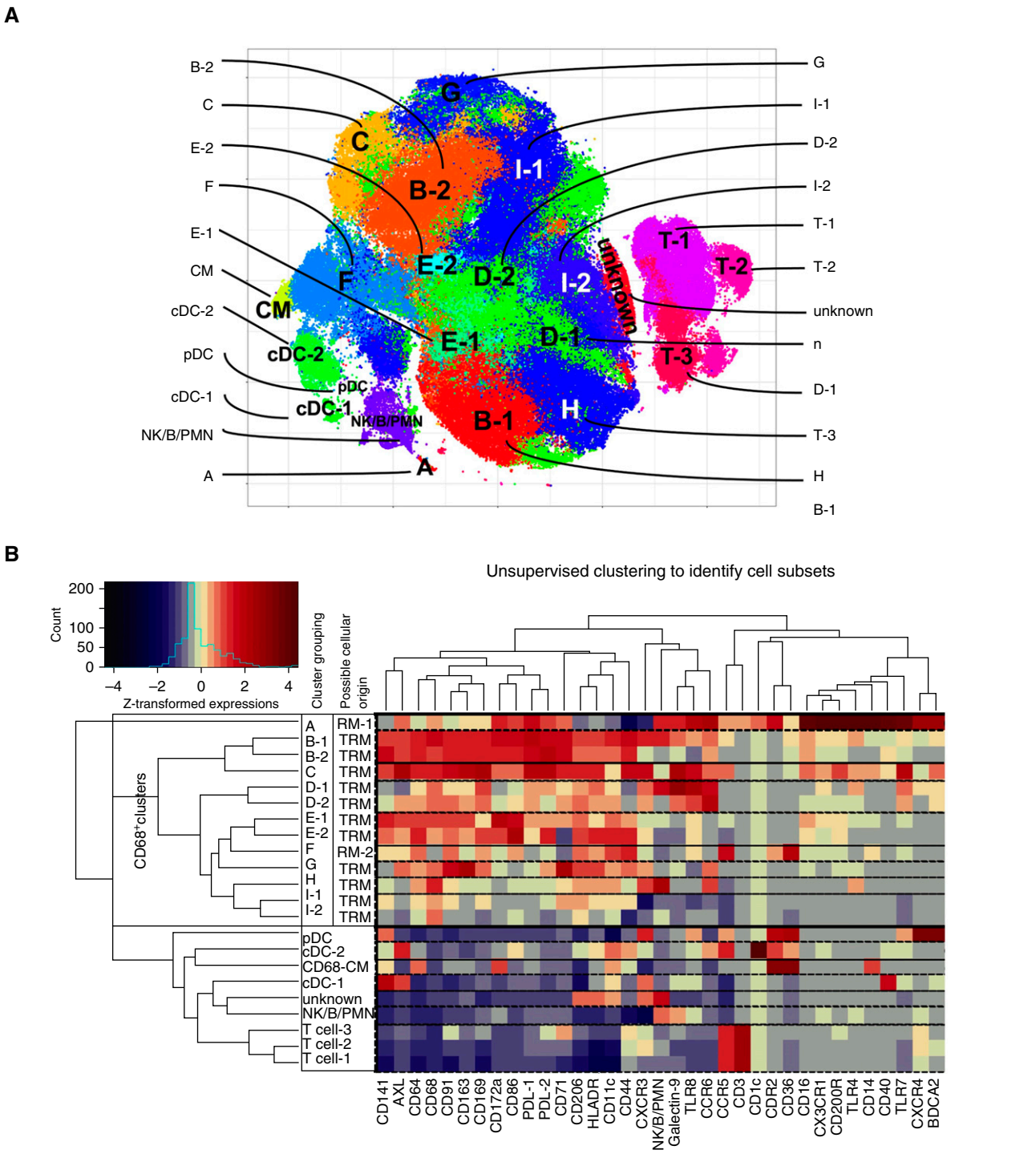

Figure 2. High-dimensional analysis of BAL cells revealed novel subtypes of myeloid cells. (*A*) CD45$^+$ immune cells from all subjects ($n = 32$ samples) were analyzed using t-distributed stochastic neighbor embedding (tSNE) dimension reduction algorithm and were found to be composed of 22 different clusters. (*B*) Heatmap of hierarchical clustering of the median intensities of markers ($n = 35$ markers) and Rphenograph-generated clusters ($n = 22$ clusters) were grouped and annotated on the basis of dendrograms and marker expression. The clusters that are CD68$^+$ (macrophages) are highlighted within the black box. cDC = conventional dendritic cell; CM = classical monocyte; NK = natural killer; pDC = plasmacytoid dendritic cell; PMN = polymorphonuclear neutrophil; RM = recruited macrophage; TRM = tissue-resident macrophage.

cerium and lanthanum within BAL immune cells, especially in smokers (Figure E4). Channels with background signal from these contaminants were consistently identified as atomic mass 139, 140, and 142. For the remainder of our studies, we did not use channels 139 and 140 for analysis and used channel 142 only to exclude granulocytes (CD66b), natural killer (NK) cells (CD56), and B cells (CD19). Our final 39-marker panel used for this study was focused on cells of myeloid origin and is detailed in Table 2. Data acquisition, deconvolution, and manual gating performed before high-dimensional analysis are shown in Figure 1.

High-Dimensional Analysis of BAL Cells Revealed Novel Subtypes of Myeloid Cells

Previous work established phenograph as a robust method for the high-dimensional phenotypic clustering of tissue-myeloid cell populations (10). Similarly, we used this approach to analyze phenotypic data of myeloid cells from human BAL. First, tSNE-based dimension reduction of $CD45^+$ cells (Figure 2A) followed by unsupervised clustering using phenograph identified 22 immune cell clusters (Figure 2B). Expression of the tissue macrophage marker CD68 divided the clusters into two major populations consisting of 13 $CD68^+$ clusters and nine $CD68^{low/-}$ clusters that we then validated by manual gating (Figure 3A) (11). The $CD68^+$ clusters were given letter annotations (A–I) and were subdivided on the basis of dendrograms of hierarchical clustering (Figure 2B). They consisted of 11 tissue-resident macrophage (TRM) (B–E and G–I) clusters and two clusters highly expressing CCR2, which were termed "recruited macrophages" (RMs) (A and F). The nine $CD68^{low/-}$ clusters included three subsets of dendritic cells (DCs) (plasmacytoid DCs, conventional DC-2 [cDC-2], and conventional DC-1 [cDC-1]) based on the expression of BDCA-2, CD-1c, and CD141, respectively; $CCR2^+$ classical monocytes (CMs) ($CD68^-$CM); and a unique subtype of background high cells that stained positive only for CD206, CD11c, HLADR, and CXCR3, labeled as "unknown," resembling a recently described and similarly labeled subset (12). The $CD68^{low/-}$ clusters also included T cells and a mixed NK/B/polymorphonuclear neutrophil (PMN) population. The latter population identified by clustering was negative for all myeloid and T-cell markers and was considered true positive for NK/B/PMN cells.

The unsupervised clusters were then evaluated by manual gating of $CD45^+$ cells (Figure 3A). First, cells that were negative for CD206 and positive for CD56/CD19/CD66b were considered NK/B/PMN cells and were excluded. The remaining cells were divided into $CD3^+$ T cells and non-T cells. Because T cells should not express the majority of the markers on this myeloid cell–focused panel, they were used to determine the optimal placement of manual gates. Non-T cells were divided into $CD68^+$ and $CD68^-$ cells to identify DC, monocyte, RM, and TRM populations.

To assess intercluster relationships, we performed cellular progression analysis using nonlinear dimension reduction by ISOMAP, in which the distance between clusters determines their relatedness (8). Figure 3B demonstrates the overall relatedness of T-cell clusters, DC clusters, and $CD68^+$ clusters. The NK/B/PMN cluster was most closely related to the T-cell clusters, whereas the CM subset was situated between the DC and $CD68^+$ clusters. Intercluster relatedness was also assessed using linear transformation analysis by PCA, which reinforced the observations made by ISOMAP, and the cluster-groups established by hierarchical clustering.

Smoking is Associated with Higher Expression of Activation Markers and Lower Expression of Regulatory Proteins on Subtypes of Myeloid Cells

The impact of smoking on the phenotypic landscape of pulmonary myeloid cells was evaluated on samples from never-smokers and smokers without evidence of COPD. Clustered phenotypes were visualized in tSNE dimensions, which displayed a clear difference in cell density across multiple clusters between the two groups (Figure 4A). Furthermore, PCA that included cluster abundance, median marker expression within each cluster, age, and sex suggested differences between smokers and never-smokers.

A regression analysis with adjustment for age was performed to determine statistical differences in cluster abundance and marker expressions by smoking status. A lower abundance of T-cell and cDC-1 clusters were observed with smoking ($P < 0.05$; Figure 4B). There was a higher abundance of F, H, and I-2 clusters in smokers (all $P < 0.001$; Figure 4B).

Pulmonary myeloid cells from smokers had lower expression of the chemokine receptor CCR2 and a higher expression of CD68 in the RM cluster F (all $P < 0.01$; Figure 4C). Among the TRM subsets, a lower expression of AXL was seen in cluster E-2 ($P < 0.01$). A lower expression of PDL1 and CCR6 was observed on pulmonary myeloid cells from all smokers on cluster G (all $P < 0.01$). Interestingly, smoking was associated with changes in a number of markers on cluster G that were also observed on other myeloid cell clusters (CCR6, CD36, CD11c, and CD44).

Lower Expression of PDL1, PDL2, and AXL Observed on Macrophages in COPD

We next evaluated the effect of COPD on BAL myeloid cells on samples from subjects with COPD GOLD stages 2 and 3 and never-smoking control subjects without COPD. Differences in the distribution of myeloid cell clusters were visually apparent in tSNE space (Figure 5A). PCA of samples with cluster abundance, median marker expressions within clusters, age, and sex suggested differences between never-smokers without COPD and subjects with COPD. No separation was seen between GOLD stages 2 and 3 on Dim1 and Dim2 dimensions.

The cluster abundance of the unknown cluster and the RM cluster F were higher in subjects with more severe COPD compared with never-smokers without COPD ($P < 0.05$; Figure 5B). The B-2 cluster ($P < 0.001$) was found in lower abundance in COPD, whereas the B-1 cluster was higher in abundance with COPD GOLD stage 2 ($P < 0.05$; Figure 5B). The H and I-2 clusters were also higher in COPD GOLD stage 2 after adjustment for smoking status ($P < 0.01$; Figure 5B).

Although the expression of some markers was associated with COPD in general, the expression of others seems to be affected by the severity of COPD, as determined by GOLD stage. For example, lower expression of CCR6 was observed on pulmonary myeloid cells in F and I-1 clusters with more severe COPD (all $P < 0.01$; Figure 5C). The expression of PDL1 and PDL2

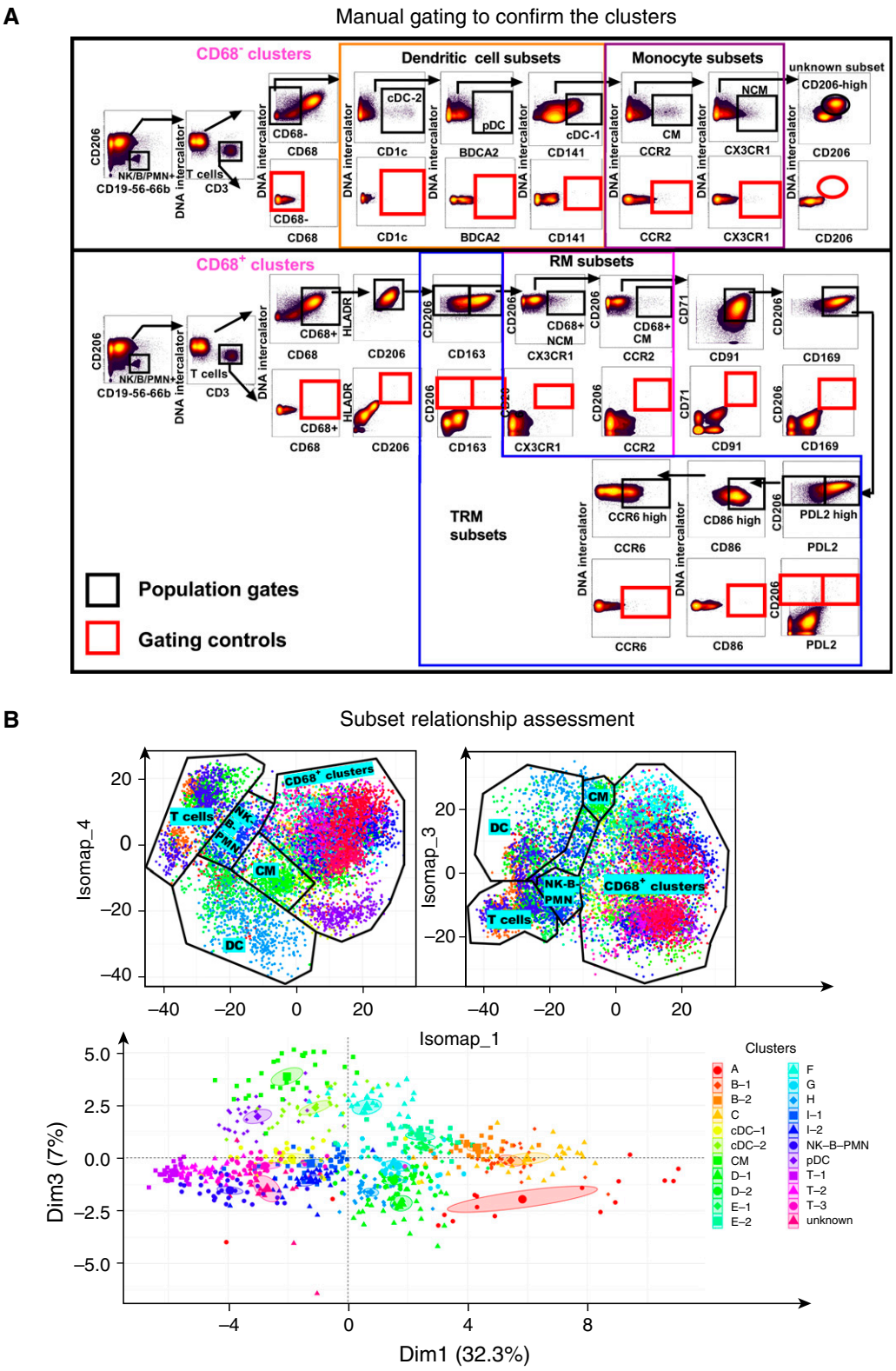

Figure 3. Confirmation of identified populations and their intercluster relationship. (*A*) Two-dimensional scatter graphs from a representative sample are shown for manual gating and confirmation of identified cell subpopulations of $CD68^{-}$ and $CD68^{+}$ clusters. The gating controls are based on the same population in T cells (red box) and are shown below the identified populations (black box). RM subsets denote the likely RMs, whereas TRM subsets denote the likely TRMs. (*B*) The intercluster relationship assessed by isometric feature mapping (Isomap) and principal component analysis (PCA) are shown.

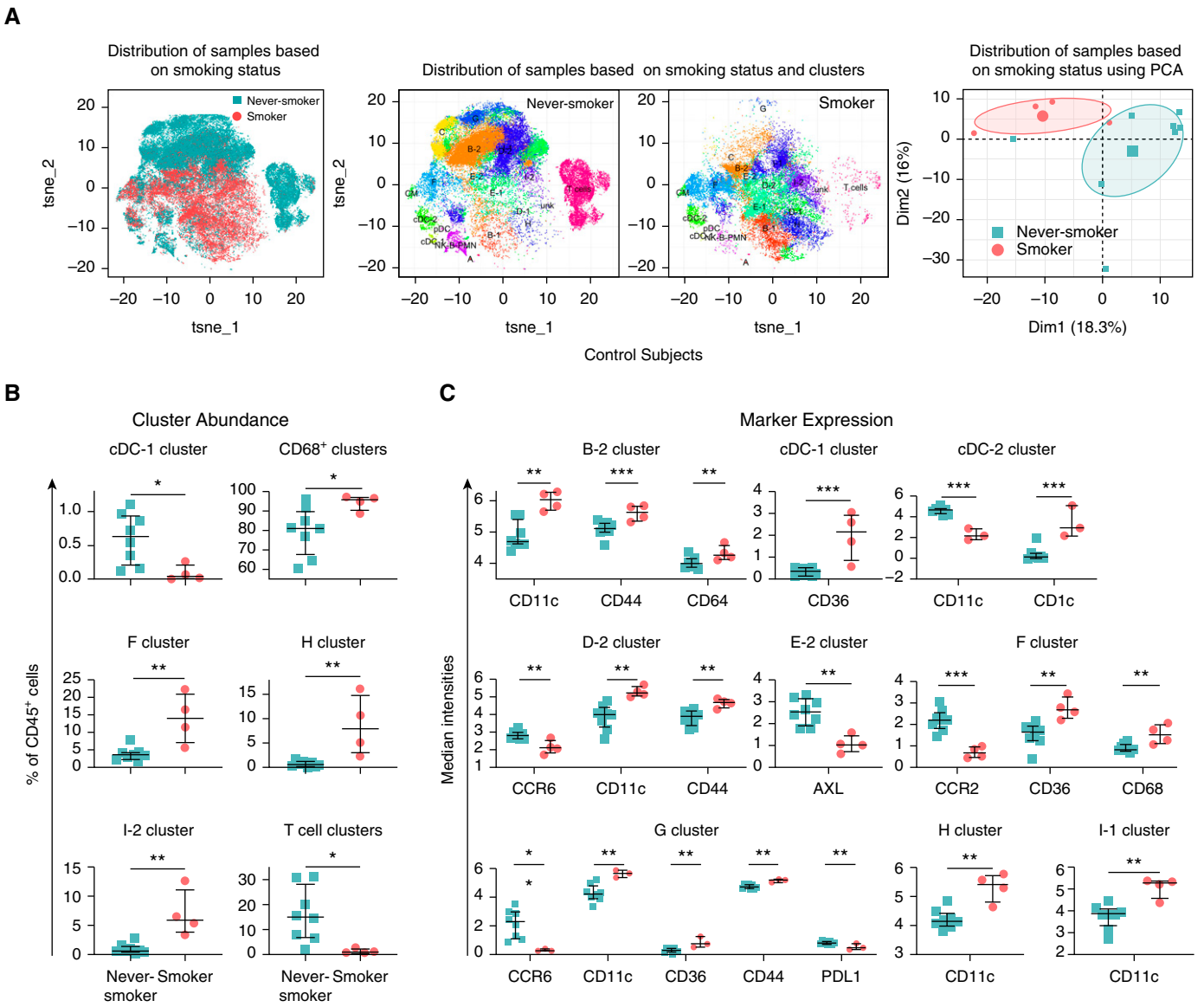

Figure 4. Smoking is associated with higher expression of activation markers and lower expression of regulatory proteins on subtypes of myeloid cells. (*A*) Cell density in samples from never-smokers ($n = 8$) and current smokers ($n = 4$) among control subjects without COPD are shown in tSNE dimensions and are separated on the basis of smoking status to show overall change in clusters. Distribution of samples based on smoking status using PCA for marker expression, cluster abundance, age, and sex parameters in Dim1 (PC1) and Dim2 (PC2) dimensions are shown. (*B*) Percentage of $CD45^+$ cells in never-smokers (circles; $n = 8$) and current smokers (squares; $n = 4$) among control subjects for significantly different clusters are shown. (*C*) Median intensities of differentially expressed markers between never-smokers (circles; $n = 8$) and current smokers (squares; $n = 4$) among control subjects for significantly different clusters are shown. For *B* and *C*, plots represent the median and interquartile range. Only statistically significant comparisons are shown. Statistical significance was defined on the basis of regression modeling and after Benjamini-Hochberg correction for multiple comparisons. The *P* values presented are from regression modeling without correction. $^*P \leq 0.05$, $^{**}P \leq 0.01$, and $^{***}P \leq 0.001$.

within F and I-1 clusters was also lower on cells from patients with more severe COPD (all $P < 0.01$). Similarly, the expression of the tyrosine kinase receptor AXL was lower on clusters E-2 and I-1 with more severe COPD (all $P < 0.01$). Moreover, PDL2 had a lower expression in clusters cDC-2 and I-2 in more severe COPD (all $P < 0.001$). In contrast, CCR6 had a lower expression in cluster G in all patients with COPD, and CD86 and TLR8 had higher expressions in B-2 cluster in patients with GOLD stage 2 (all $P < 0.01$; Figure 5C). Overall, RM cluster F, TRM cluster I-1, and cDC-2 showed the most evidence of COPD-associated immune modulation.

To determine the effect of current smoking, the abundance of clusters in subjects with COPD was analyzed after stratification by smoking status. This analysis showed that D-2 cluster abundance was higher in current smokers ($P < 0.01$; Figure 6) after adjustment for covariates. In addition, the use of inhaled corticosteroids did not have an effect on immune cell

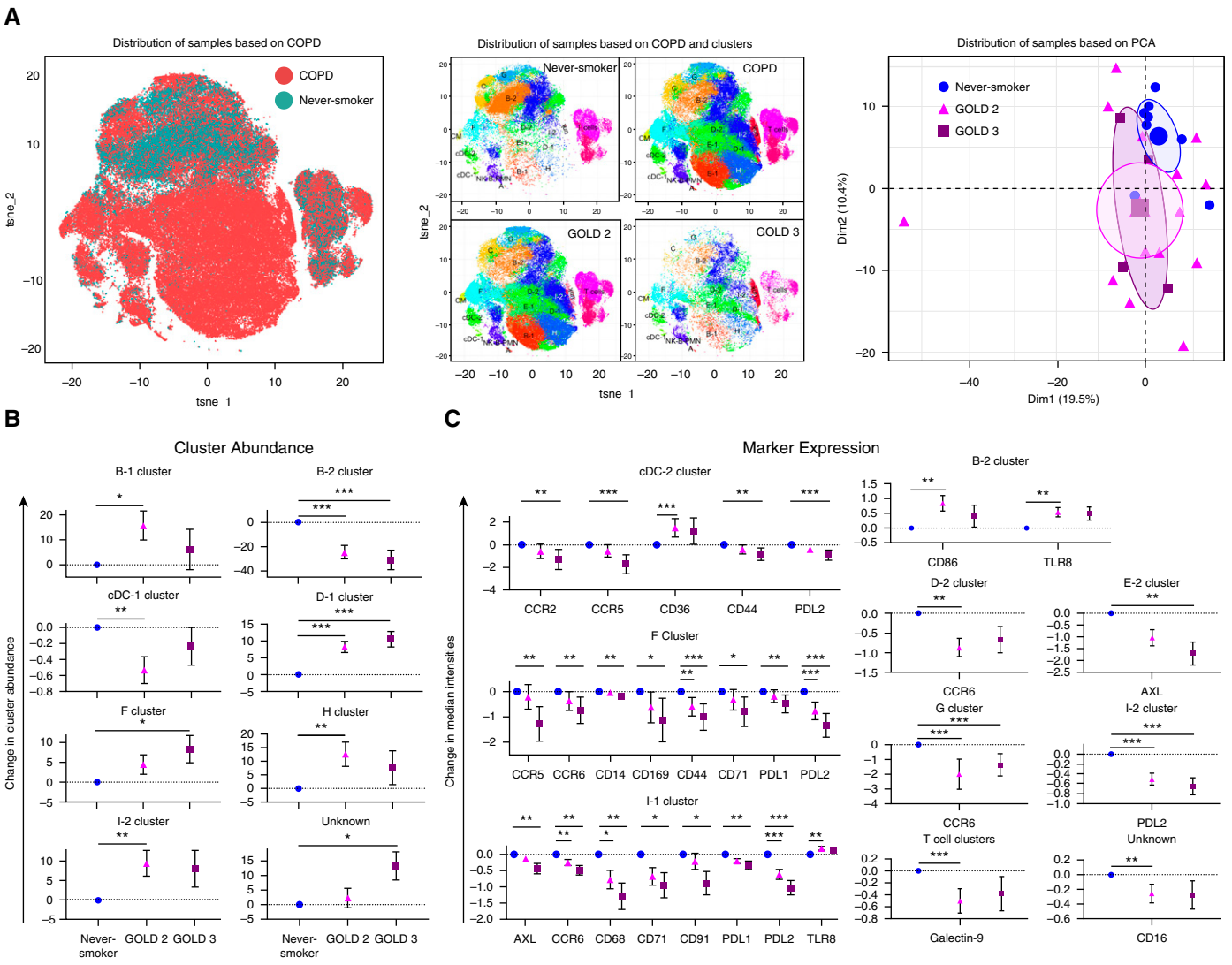

Figure 5. Lower expression of PDL1, PDL2, and AXL observed on macrophages in COPD. (*A*) Cell density in samples from never-smokers without COPD ($n = 8$) and subjects with COPD ($n = 20$) are shown in tSNE dimensions and are separated on the basis of COPD status to show overall change in clusters. Distribution of samples based on COPD Global Initiative on Obstructive Lung Disease (GOLD) stages using PCA for marker expression, cluster abundance, age and sex parameters in Dim1 (PC1) and Dim2 (PC2) dimensions are shown. (*B*) Change in cluster abundance from never-smokers without COPD (reference) (circle; $n = 8$) with GOLD stage 2 (triangle; $n = 16$) and GOLD stage 3 (square; $n = 4$) for significantly different clusters are shown. (*C*) Change in median intensities of differentially expressed markers from never-smokers without COPD (reference) (circle; $n = 8$) with GOLD stage 2 (triangle; $n = 16$) and GOLD stage 3 (square; $n = 4$) for significantly different clusters are shown. For *B* and *C*, the dotted line represents the reference value, and plots represent estimates and confidence intervals from the regression model. Only statistically significant comparisons are shown. Statistical significance was defined on the basis of regression modeling and after Benjamini-Hochberg correction for multiple comparisons. The *P* values presented are from regression modeling without correction. $^{*}P < 0.05$, $^{**}P \leq 0.01$, and $^{***}P \leq 0.001$.

abundances or marker expression among subjects with COPD (Table E2).

Prior COPD Exacerbations Showed a Trend toward Higher Expression of CD169 on Multiple Myeloid Subtypes

We examined BAL cells obtained from subjects with COPD that were categorized as exacerbators or nonexacerbators on the basis of a confirmed history of COPD exacerbation in the preceding 3 years. Although the abundance of clusters was not different between exacerbators and nonexacerbators, the distribution of cells across the clusters was visually different in tSNE space (Figure 7A), and the expression of several markers within those clusters differed in unadjusted analysis. Within the $CD68^{-}$ CM cluster, exacerbators had a tendency for higher expression of CD169 and PDL2 (all $P < 0.05$ but BH ≥ 0.1; Figure 7B). A tendency for higher expression of CD169 was also observed in H and E-1 clusters (all $P < 0.05$ but BH ≥ 0.1). The expression of TLR4 tended to be higher within the A cluster ($P < 0.01$ but BH ≥ 0.1; Figure 7B). Within the G cluster, a tendency for lower expression of AXL and TLR7 expression was observed (all $P < 0.05$ but BH ≥ 0.1; Figure 7B).

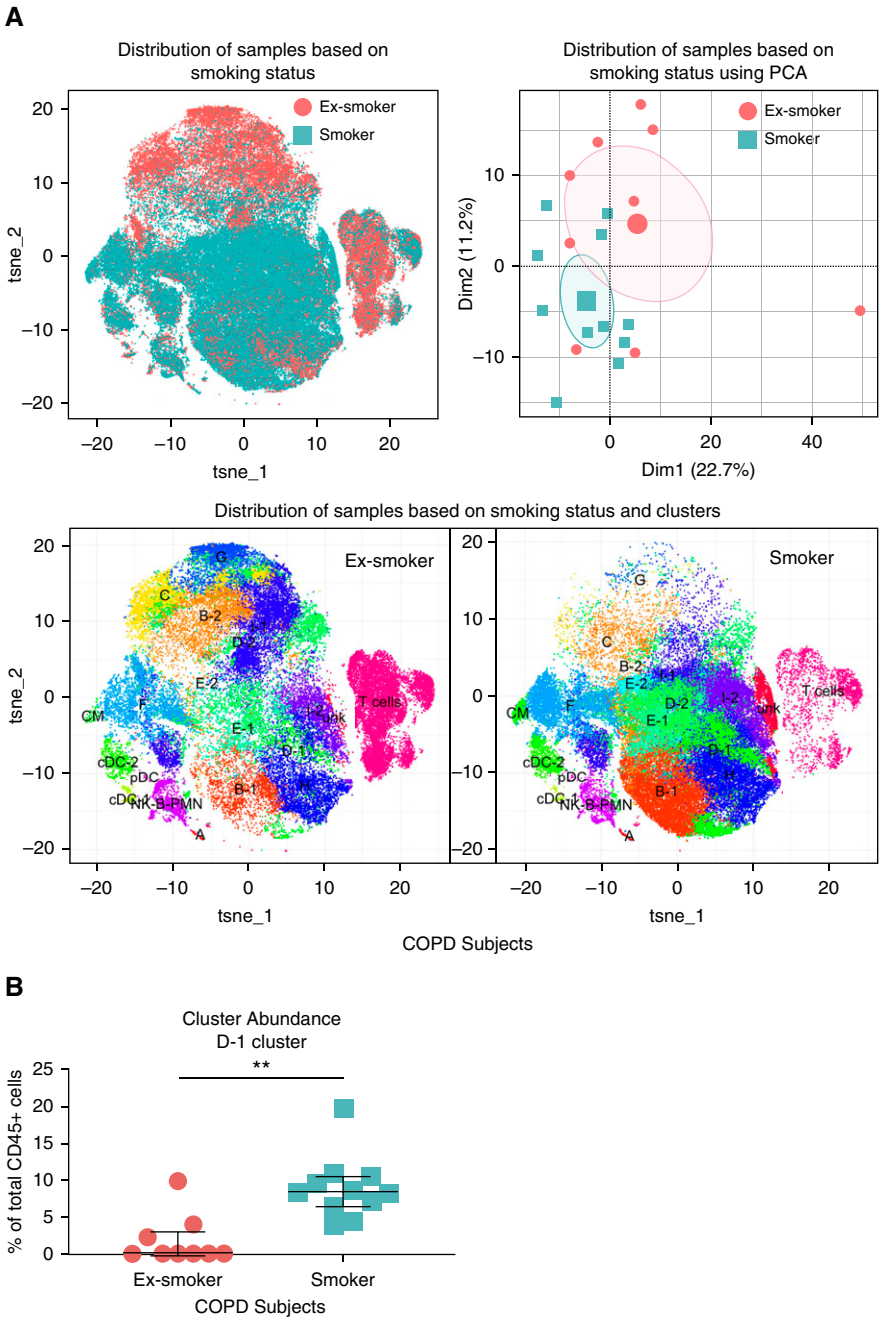

Figure 6. Effect of continued smoking on immune cells in BAL cells from patients with COPD. (*A*) Cell density in samples from ex-smokers (circles; $n = 9$) and smokers (squares; $n = 11$) among subjects with COPD are shown in tSNE dimensions and are separated on the basis of smoking status to show overall change in clusters. Distribution of samples based on smoking status using PCA for marker expression, cluster abundance, age, and sex parameters in Dim1 (PC1) and Dim2 (PC2) dimensions are shown. (*B*) Percentage of $CD45^+$ cells in ex-smokers (circles; $n = 9$) and smokers (squares; $n = 11$) among subjects with COPD for the (*A*) D-1 cluster is shown. For *B*, the plot represents the median and interquartile range. The comparison shown was the only statistically significant comparison. Statistical significance was defined on the basis of regression modeling and after Benjamini-Hochberg correction for multiple comparisons. The *P* values presented are from regression modeling without correction. $^{**}P < 0.01$.

Discussion

The aim of our study was to evaluate the immunophenotypic changes on pulmonary myeloid cells associated with smoking and COPD. Using mass cytometry, we assessed cells from the BAL of smokers and nonsmokers with or without COPD and patients with COPD with or without a history of exacerbations. We identified major populations of $CD68^+$ and $CD68^-$ cells with 22 distinct phenotypic clusters, of which 18 were myeloid cell subtypes including 11 TRMs, three DCs, three monocyte/possibly RMs, and one $CD206^+CD68^-$ unknown cluster. Smoking and COPD were found to be associated with higher abundance of RMs and with phenotypic changes in TRMs, suggesting a bias toward macrophage subtypes of proinflammatory state.

There are limited CyTOF-based studies examining changes in pulmonary myeloid cells with disease. Interestingly, the only other BAL CyTOF study in disease that examined patients with acute respiratory distress syndrome showed similar myeloid cell diversity, such as the expression of PDL1 among TRM clusters that could be further stratified by the expression of CD169 (12). We identified three distinct subtypes of $PDL1^{high}/CD169^{high}$ cells (B1, B2, and C) in patients with COPD. Cluster B1 was increased and cluster B2 was decreased with COPD severity. Also, we found that $PDL1^{low}/CD169^{low}/CCR6^+$ (cluster H) and $PDL1^{int}/CD169^{int}/CCR6^+$ (cluster D-1) cells were increased in BAL with smoking and/or COPD. As prior observations of $PDL1^{low}/CD169^{low}/CD206^+$ (such as cluster H) cells have indicated that these cells localize to the interstitium of healthy donors (13), our findings reinforce the idea that $CCR6^+$ cells are recruited to sites of epithelial inflammation mediated by CCR6–CCL20 interactions (14).

The recruitment of pulmonary myeloid cells is a hallmark of COPD (15). We assessed populations of recruited myeloid cells by evaluating the relative expression of homing receptors (i.e., CC and CX receptors) versus that of markers associated with tissue residency (e.g., CD163, CD68,

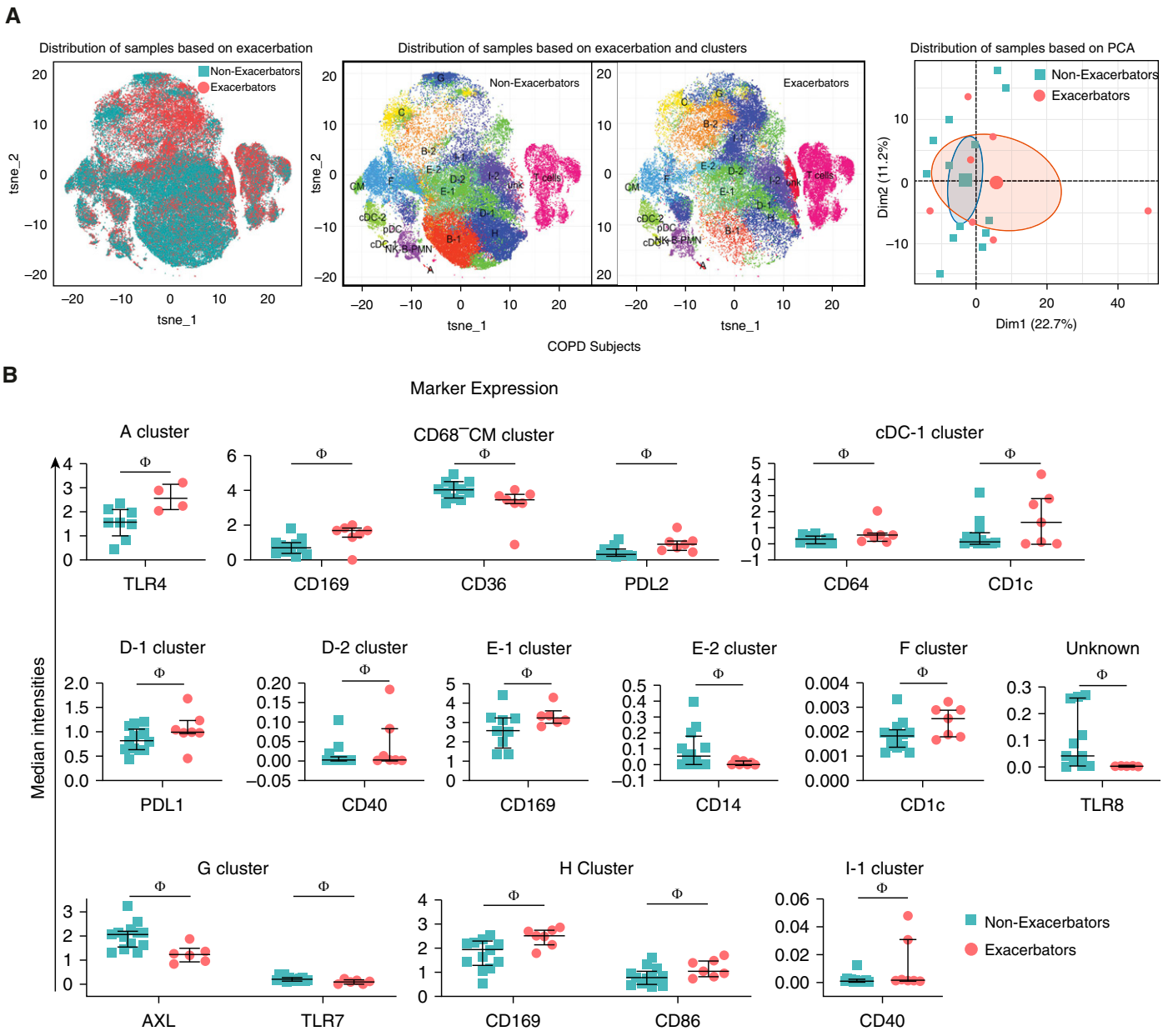

Figure 7. Prior COPD exacerbations showed a trend toward higher expression of CD169 on multiple myeloid subtypes. (*A*) Cell density in samples from nonexacerbators ($n = 13$) and exacerbators ($n = 7$) among subjects with COPD are shown in tSNE dimensions and are separated on the basis of exacerbation status to show overall change in clusters. Distribution of samples based on exacerbation status using PCA for marker expression, cluster abundance, age, and sex parameters in Dim1 (PC1) and Dim2 (PC2) dimensions are shown. (*B*) Median intensities of differentially expressed markers between nonexacerbators (circles; $n = 13$) and exacerbators (squares; $n = 7$) among subjects with COPD for significantly different clusters (uncorrected for multiple comparisons) are shown. The plots represent the median and interquartile range. The *P* values presented are from regression modeling without Benjamini-Hochberg correction. $^{\Phi}$Uncorrected $P < 0.05$.

and CD206; Figure E5). It is known that CCR2 is associated with migration across vasculature (16), CXCR4 is associated with egress from the bone marrow (17), and CX3CR1, CCR5/6, and CXCR3 are associated with migration across tissues (18, 19). Thus, we expected recent myeloid cell arrivals to the lung from the vasculature to be $CCR2^{high}$ with low concentrations of tissue residency markers that would change over time as cells established residency in the lung.

Although the $CD68^{+}$ CM (cluster F) subtype of RMs was higher in abundance in both smokers without COPD and subjects with severe COPD, $CD68^{+}$ CMs from these two groups of patients showed distinct differences in marker expression. Smokers had lower CCR2 expression and higher CD68 expression on this subtype compared with never-smokers. This phenotype would be expected on cells migrating from the interstitium rather than cells recently recruited from the blood. With increased

severity of COPD, we observed decreased expression of CCR5 and CCR6 on $CD68^+$ CMs, which is consistent with cells migrating from the vasculature. These changes also correlated with lower expression of CD169, suggesting recent migration of cells to the airway (20). Thus, COPD with or without smoking may lead to increased $CD68^+$ CMs, which are likely recruited from the peripheral circulation, whereas smoking, in the absence of COPD, led to increased $CD68^+$ CMs, which are likely recruited more locally from the interstitium.

In addition to signatures of cellular migration, we observed other changes in myeloid cell subtypes from COPD. Importantly, we observed that multiple myeloid subtypes among patients with COPD (I-1 and E-2) and those with past COPD exacerbations (G) displayed lower expression of AXL, a receptor known to play a role in efferocytosis and the regulation of the NLRP3 inflammasome (21, 22). AXL has been the main apoptotic cell recognition receptor found expressed on human BAL macrophages (23). Reduced AXL expression is suggested to perpetuate chronic inflammation (23). For example, the inhibition of AXL is associated with the progression of asthma (23). AXL has also been proposed to play a role in the pathogenesis of COPD (23–25), although evidence for that role in humans is lacking. Our study provides new information about the differential expression of AXL on myeloid subsets in the setting of COPD.

COPD was also associated with lower expression of PDL1 and/or PDL2 on several clusters of macrophages. Although a lower abundance of one $PDL1/2^{high}$ cluster (B-2) was seen, another smaller $PDL1/2^{high}$ (B-1) cluster was found to have a higher abundance in COPD. Within the B-2 cluster, activation markers (CD86 and TLR8) were higher on cells from patients with COPD, suggesting a more activated myeloid subtype in COPD. In addition, we found that COPD was associated with lower expression of galectin-9 on T cells. Because others have demonstrated that inhibition of T-cell responses may be mediated by galectin-9 expression, our observations suggest a lower threshold for T-cell immune activation in COPD (26, 27). Finally, three myeloid cell clusters from exacerbators were noted to have a tendency for higher expression of CD169, a marker believed to bind sialylated viruses and bacteria (28). Thus, the tendency for higher expression of CD169 on cells from exacerbators may imply an increased potential for activation and inflammation upon exposure to invading pathogens, which may then contribute to episodes of exacerbation.

In addition to the TRM and RM subsets, our work also clarifies prior CyTOF-based studies of DC subsets in BAL (25, 28, 29) and informs the origin and migration of DCs to the lung. First, plasmacytoid DCs expressed high concentrations of CXCR4 and CCR2, confirming their established origin from the bone marrow (30). Interestingly, the cDC-1 and cDC-2 subtypes we observed corresponded with recently identified AXL^+ DCs (31–34). In previous reports, well-differentiated AXL^+ cDCs were gated on $CD141^-$ cells (33). By contrast, our subtypes were $CD141^+$, consistent with observations that with maturation, AXL expression decreases on both cDC-1 and cDC-2 subtypes, whereas CD141 expression decreases along cDC-2 differentiation but remains high on cDC-1 cells (32, 34, 35). Accordingly, we observed that the cDC-1 subtype had higher expression of CD141 compared with the cDC-2 subtype; however, the cDC-2 subtype displayed intermediate expression of CD141 and intermediate/high expression of CCR2, representing a cDC-2 population made up of immature progenitors from the circulation. These observations are summarized in Figure E6, which describes a proposed model of marker expression on the subsets of recruited myeloid cells after their migration into lung tissue and airways.

Our CyTOF-based immunophenotyping study of myeloid cells provides a number of useful observations about the impact of smoking and COPD on airway immune cells; however, limitations of this work should be noted. Although CyTOF was able to bypass autofluorescence, contamination of pulmonary myeloid cells with heavy-metal isotopes of cerium and lanthanum could produce spurious results in certain channels. However, this challenge was addressed by avoiding affected channels, evaluating unstained control samples, and using affected channels as dump channels for excluded cells and controls for metal contamination (e.g., channels 139, 140, and 142). The small sample size of the study impacted our capacity to perform detailed subgroup analysis across multiple clinical phenotypes and treatment regimens. Notably, some differences found in marker expression associated with a history of exacerbation were not significant after adjusting for multiple comparisons. Finally, the ability to identify differences associated with severity of exacerbation was limited because the subjects we examined were not frequent exacerbators (usually defined as $\geq$2 exacerbations per year). Despite these limitations, our findings highlight the strength of CyTOF-based deep phenotyping to evaluate the diverse myeloid cell populations in a heterogenous disease such as COPD.

To conclude, this study provides novel evidence for the impact of smoking and COPD on airway myeloid cells and demonstrates that COPD is associated with an increase in likely RMs in BAL and in an increase in subtypes with decreased regulation of inflammation together with an increase in expression of proinflammatory markers. Our data also suggest a decrease in regulatory proteins (PDL1, PDL2, and AXL) in myeloid cells, which may be contributing to the chronic inflammation seen in COPD. Importantly, this study expands the field of COPD and myeloid immunobiology by establishing a framework to evaluate airway myeloid subpopulations for future studies involving disease progression and treatment response. ■

Author disclosures are available with the text of this article at www.atsjournals.org.

Acknowledgment: The authors thank the study participants, research staff, and San Francisco Veterans Affairs clinical staff for making this research possible. They also thank Mr. Joseph Doherty for bronchoscopy assistance, former and current clinical coordinators in the Arjomandi Laboratory for subject recruitment and database management, and Drs. Christine Hsieh and James Ryan for helpful discussions. They also thank the UCSF, single-cell analysis and time of flight mass cytometry core for assistance with mass cytometry experiments.

References

1. World Health Organization. Chronic obstructive pulmonary disease. Geneva, Switzerland: World Health Organization; 2017 [accessed 2019 Oct 6]. Available from: https://www.who.int/news-room/fact-sheets/detail/chronic-obstructive-pulmonary-disease-(copd).
2. Morales-Nebreda L, Misharin AV, Perlman H, Budinger GR. The heterogeneity of lung macrophages in the susceptibility to disease. *Eur Respir Rev* 2015;24:505–509.
3. Barnes PJ, Shapiro SD, Pauwels RA. Chronic obstructive pulmonary disease: molecular and cellular mechanisms. *Eur Respir J* 2003;22: 672–688.
4. Sköld CM, Hed J, Eklund A. Smoking cessation rapidly reduces cell recovery in bronchoalveolar lavage fluid, while alveolar macrophage fluorescence remains high. *Chest* 1992;101: 989–995.
5. Hodge SJ, Hodge GL, Holmes M, Reynolds PN. Flow cytometric characterization of cell populations in bronchoalveolar lavage and bronchial brushings from patients with chronic obstructive pulmonary disease. *Cytometry B Clin Cytom* 2004;61:27–34.
6. Arjomandi M, Witten A, Abbritti E, Reintjes K, Schmidlin I, Zhai W, *et al*. Repeated exposure to ozone increases alveolar macrophage recruitment into asthmatic airways. *Am J Respir Crit Care Med* 2005; 172:427–432.
7. Crapo RO, Morris AH, Gardner RM. Reference spirometric values using techniques and equipment that meet ATS recommendations. *Am Rev Respir Dis* 1981;123:659–664.
8. Chen H, Lau MC, Wong MT, Newell EW, Poidinger M, Chen J. Cytofkit: a Bioconductor package for an integrated mass cytometry data analysis pipeline. *PLOS Comput Biol* 2016;12:e1005112.
9. Böhlandt A, Schierl R, Diemer J, Koch C, Bolte G, Kiranoglu M, *et al*. High concentrations of cadmium, cerium and lanthanum in indoor air due to environmental tobacco smoke. *Sci Total Environ* 2012;414: 738–741.
10. Levine JH, Simonds EF, Bendall SC, Davis KL, Amir AD, Tadmor MD, *et al*. Data-driven phenotypic dissection of AML reveals progenitor-like cells that correlate with prognosis. *Cell* 2015;162: 184–197.
11. Chistiakov DA, Killingsworth MC, Myasoedova VA, Orekhov AN, Bobryshev YV. CD68/macrosialin: not just a histochemical marker. *Lab Invest* 2017;97:4–13.
12. Morrell ED, Wiedeman A, Long SA, Gharib SA, West TE, Skerrett SJ, *et al*. Cytometry TOF identifies alveolar macrophage subtypes in acute respiratory distress syndrome. *JCI Insight* 2018;3:e99281.
13. Yu Y-RA, Hotten DF, Malakhau Y, Volker E, Ghio AJ, Noble PW, *et al*. Flow cytometric analysis of myeloid cells in human blood, bronchoalveolar lavage, and lung tissues. *Am J Respir Cell Mol Biol* 2016;54:13–24.
14. Ito T, Carson WF IV, Cavassani KA, Connett JM, Kunkel SL. CCR6 as a mediator of immunity in the lung and gut. *Exp Cell Res* 2011;317: 613–619.
15. Traves SL, Smith SJ, Barnes PJ, Donnelly LE. Specific CXC but not CC chemokines cause elevated monocyte migration in COPD: a role for CXCR2. *J Leukoc Biol* 2004;76:441–450.
16. Fantuzzi L, Borghi P, Ciolli V, Pavlakis G, Belardelli F, Gessani S. Loss of CCR2 expression and functional response to monocyte chemotactic protein (MCP-1) during the differentiation of human monocytes: role of secreted MCP-1 in the regulation of the chemotactic response. *Blood* 1999;94: 875–883.
17. Shen H, Cheng T, Olszak I, Garcia-Zepeda E, Lu Z, Herrmann S, *et al*. CXCR-4 desensitization is associated with tissue localization of hemopoietic progenitor cells. *J Immunol* 2001;166: 5027–5033.
18. Zhang J, Patel JM. Role of the CX3CL1-CX3CR1 axis in chronic inflammatory lung diseases. *Int J Clin Exp Med* 2010;3: 233–244.
19. Mantovani A, Sica A, Sozzani S, Allavena P, Vecchi A, Locati M. The chemokine system in diverse forms of macrophage activation and polarization. *Trends Immunol* 2004;25: 677–686.
20. Bharat A, Bhorade SM, Morales-Nebreda L, McQuattie-Pimentel AC, Soberanes S, Ridge K, *et al*. Flow cytometry reveals similarities between lung macrophages in humans and mice. *Am J Respir Cell Mol Biol* 2016;54:147–149.
21. Han J, Bae J, Choi CY, Choi SP, Kang HS, Jo EK, *et al*. Autophagy induced by AXL receptor tyrosine kinase alleviates acute liver injury via inhibition of NLRP3 inflammasome activation in mice. *Autophagy* 2016;12:2326–2343.
22. Cross SN, Potter JA, Aldo P, Kwon JY, Pitruzzello M, Tong M, *et al*. Viral infection sensitizes human fetal membranes to bacterial lipopolysaccharide by MERTK inhibition and inflammasome activation. *J Immunol* 2017;199:2885–2895.
23. Grabiec AM, Denny N, Doherty JA, Happonen KE, Hankinson J, Connolly E, *et al*. Diminished airway macrophage expression of the Axl receptor tyrosine kinase is associated with defective efferocytosis in asthma. *J Allergy Clin Immunol* 2017;140: 1144–1146, e4.
24. Grabiec AM, Hussell T. The role of airway macrophages in apoptotic cell clearance following acute and chronic lung inflammation. *Semin Immunopathol* 2016;38:409–423.
25. Fujimori T, Grabiec AM, Kaur M, Bell TJ, Fujino N, Cook PC, *et al*. The Axl receptor tyrosine kinase is a discriminator of macrophage function in the inflamed lung. *Mucosal Immunol* 2015;8: 1021–1030.
26. Oomizu S, Arikawa T, Niki T, Kadowaki T, Ueno M, Nishi N, *et al*. Cell surface galectin-9 expressing Th cells regulate Th17 and Foxp3^{+} Treg development by galectin-9 secretion. *PLoS One* 2012;7: e48574.
27. Lai J-H, Luo S-F, Wang M-Y, Ho L-J. Translational implication of galectin-9 in the pathogenesis and treatment of viral infection. *Int J Mol Sci* 2017;18:2108.
28. Macauley MS, Crocker PR, Paulson JC. Siglec-mediated regulation of immune cell function in disease. *Nat Rev Immunol* 2014;14: 653–666.
29. Baharom F, Thomas S, Rankin G, Lepzien R, Pourazar J, Behndig AF, *et al*. Dendritic cells and monocytes with distinct inflammatory responses reside in lung mucosa of healthy humans. *J Immunol* 2016;196:4498–4509.
30. Vanbervliet B, Bendriss-Vermare N, Massacrier C, Homey B, de Bouteiller O, Brière F, *et al*. The inducible CXCR3 ligands control plasmacytoid dendritic cell responsiveness to the constitutive chemokine stromal cell-derived factor 1 (SDF-1)/CXCL12. *J Exp Med* 2003;198:823–830.
31. Alcantara-Hernandez M, Leylek R, Wagar LE, Engleman EG, Keler T, Marinkovich MP, *et al*. High-dimensional phenotypic mapping of human dendritic cells reveals interindividual variation and tissue specialization. *Immunity* 2017;47: 1037–1050, e6.
32. See P, Dutertre CA, Chen J, Günther P, McGovern N, Irac SE, *et al*. Mapping the human DC lineage through the integration of high-dimensional techniques. *Science* 2017;356:eaag3009.
33. Villani AC, Satija R, Reynolds G, Sarkizova S, Shekhar K, Fletcher J, *et al*. Single-cell RNA-seq reveals new types of human blood dendritic cells, monocytes, and progenitors. *Science* 2017;356:eaah4573.
34. Rhodes JW, Tong O, Harman AN, Turville SG. Human dendritic cell subsets, ontogeny, and impact on HIV infection. *Front Immunol* 2019;10:1088.
35. Collin M, Bigley V. Human dendritic cell subsets: an update. *Immunology* 2018;154:3–20.